cmgh
CELLULAR AND MOLECULAR GASTROENTEROLOGY AND HEPATOLOGY

RESEARCH LETTER

Targeted Intestinal Tight Junction Hyperpermeability Alters the Microbiome, Behavior, and Visceromotor Responses

Markedly increases in intestinal permeability occur in inflammatory bowel disease, graft-versus-host disease, celiac disease, and multiple organ dysfunction. In these diseases, effectors of increased permeability include immune signaling,[1] microbiome,[2] and corticosteroids[3] that, in part, signal through epithelial myosin light chain kinase (MLCK). More modest permeability increases occur in other disorders, including irritable bowel syndrome (IBS), autism spectrum disorder, depression, and stress-related disorders. However, data directly linking barrier loss to phenotypes of these diseases are lacking.

To define the impact of modestly increased intestinal permeability, we studied transgenic mice with intestinal epithelial-specific constitutively-active myosin light chain kinase (CAMLCK) expression. This MLCK-dependent tight junction regulation increased intestinal permeability (Supplementary Figure S1*A* and *B*).[1] Nevertheless, postnatal growth (Supplementary Figure S1*C*), reproduction, intestinal transit (Supplementary Figure S1*D*), intestinal histology, epithelial proliferation (a sensitive indicator of epithelial damage), and epithelial turnover are unaffected in CAMLCK transgenic (*CAMLCK*^{Tg}) mice.[1] In contrast, mucosal tumor necrosis factor-α, interferon-γ, interleukin (IL)-10, and IL-13 transcripts as well as numbers of lamina propria neutrophils, CD4^{+} T cells, and IgA^{+} plasma cells are modestly increased by CAMLCK expression.[1,2] Subclinical inflammation is, therefore, present and, by microbiome-dependent, IL-17–mediated processes, affords partial protection from acute pathogen invasion.[2] Immune activation is nevertheless unlikely to amplify CAMLCK-driven permeability increases, as barrier function and ZO-1 anchoring are both acutely normalized by enzymatic MLCK inhibition.[1,4]

We initially analyzed the gut microbiome of 31 wild-type (WT) and *CAMLCK*^{Tg} pups born to 8 WT dams. The microbiomes segregated by pup genotype but not dam (Supplementary Figure S1*E*) and included increased *Clostridium* and decreased Bacteroidetes, *Enterococcus spp,* and *Prevotella* in *CAMLCK*^{Tg} mice (Supplementary Figure S1*F*). Increased intestinal permeability can therefore cause dysbiosis-like microbiome shifts. Interestingly, maternal separation, which increases intestinal permeability, causes similar alterations and can be partially corrected by MLCK inhibitor–induced barrier restoration.[5]

Microbiome alterations overlapping with the above have been reported in IBS and autism spectrum disorder. We therefore asked if *CAMLCK*^{Tg} mice displayed anxiety-like behavior, as occurs in those disorders, using the open field test (Figure 1*A*). Both the percentage of distance traveled in the center and the fraction of time spent in the center of the open field were reduced in *CAMLCK*^{Tg} mice (Figure 1*A*); this did not reflect reduced locomotor activity, as total distance traveled in the entire area was similar in *CAMLCK*^{Tg} and WT mice (Figure 1*A*). These data are consistent with increased anxiety-like behavior in *CAMLCK*^{Tg} mice. Although the results cannot differentiate between direct effects of increased permeability and those requiring intermediate mediators, these data demonstrate that intestinal permeability increases can trigger behavioral changes.

Stress and increased permeability have been associated with enhanced visceral sensitivity in humans and rodents. Surprisingly, *CAMLCK*^{Tg} mice displayed striking visceral analgesia to colorectal distension relative to WT

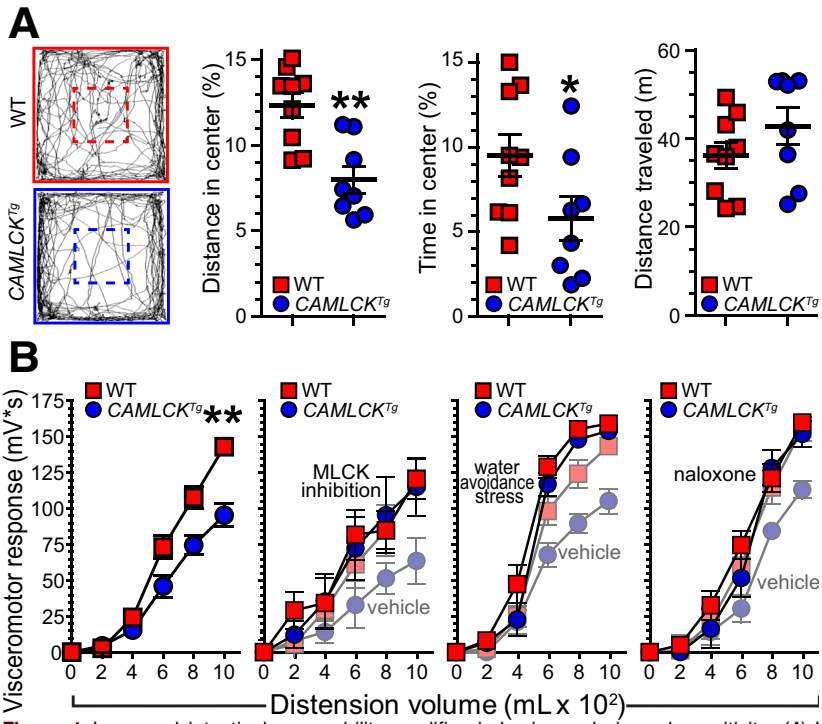

Figure 1. Increased intestinal permeability modifies behavior and visceral sensitivity. (*A*) Video-tracking paths of representative WT and *CAMLCK*^{Tg} mice in the open field test. Percent distance traveled in the center (dashed lines), percent time in the center, and overall distance traveled in the entire field are shown. *CAMLCK*^{Tg} (blue circles, n = 8) and WT (red squares, n = 9) littermates were tested. Values are mean ± SEM. *$P < .05$; **$P < .01$, Mann-Whitney *U* test. (*B*) Stepwise colorectal distension-induced visceromotor responses in *CAMLCK*^{Tg} (blue circles, n = 7) were reduced relative to WT (red squares, n = 7) littermates. Genotype-specific differences were eliminated by MLCK inhibition, water avoidance stress, or naloxone treatment. n = 5–9 per condition; for each treatment (vehicle control *CAMLCK*^{Tg} and WT mice from the same experiment are shown with pale symbols in the last three graphs). Values are mean ± SEM. **, $P < .01$, 2-way analysis of variance.

littermates (Figure 1*B*). Sensitivity was restored by enzymatic MLCK inhibition, water avoidance stress, or naloxone-mediated opioid receptor antagonism (Figure 1*B*). Although this effect of increased permeability on visceral sensitivity was unexpected, it is remarkably similar to the naloxone-reversible visceral analgesia reported in chronically stressed female rats[6] and naloxone-sensitive inhibition of nociceptive neurons by supernatants of colitic human and murine tissues.[7]

Studies of female IBS patients have linked increased permeability to altered functional and structural brain connectivity.[8] Thus, although responses to colorectal distension can be mediated by spinal reflexes as well as sensory, limbic, and paralimbic regions of the brain,[9] we asked if neuronal activation was modified by CAMLCK-induced permeability increases. C-Fos immunolabeling, an indicator of neuronal activity, was significantly greater in the paraventricular nucleus of the thalamus, the paraventricular nucleus of the hypothalamus, and the hippocampus but not the medial prefrontal cortex, nucleus accumbens, or amygdala of *CAMLCK*^{Tg}, relative to WT, mice (Figure 2, Supplementary Figure S2). Increased intestinal permeability may therefore increase basal neuronal activity in areas of the brain that regulate responses to visceral pain or stress[9] but not those associated with conscious visceral sensation.

These results demonstrate that increased intestinal permeability can impact (1) gut microbiome composition, (2) behavior, (3) visceral pain responses, and (4) neuronal activation within the brain. Critically, these changes are all results, rather than causes, of intestinal barrier loss, as the latter was induced by targeted CAMLCK expression.

The sites of neuronal activation in *CAMLCK*^{Tg} mice support the hypothesis that increased intestinal permeability can activate the hypothalamic-pituitary-adrenal axis.[10] Conversely, hypothalamic-pituitary-adrenal axis activation by exogenous stress can induce intestinal permeability increases.[3] Thus, as has been proposed in inflammatory bowel disease and graft-versus-host disease, a self-amplifying cycle may ultimately direct the diverse phenotypes induced by MLCK-dependent, intestinal permeability increases. Further study is needed to define the complex relationships between intestinal permeability, stress, behavioral alterations, visceromotor responses, microbiome composition, and other abnormalities.

These data are the first to assess behavior in a model in which a targeted increase in intestinal tight junction permeability is the only direct perturbation. The results demonstrate, unequivocally, that modest tight junction permeability increases induced via a physiologically and pathophysiologically relevant mechanism are sufficient to trigger local and systemic microbial, behavioral, and neurosensory changes. This provides a new perspective with which to understand previously hypothesized cause-effect relationships that have been proposed on the basis of correlative data.

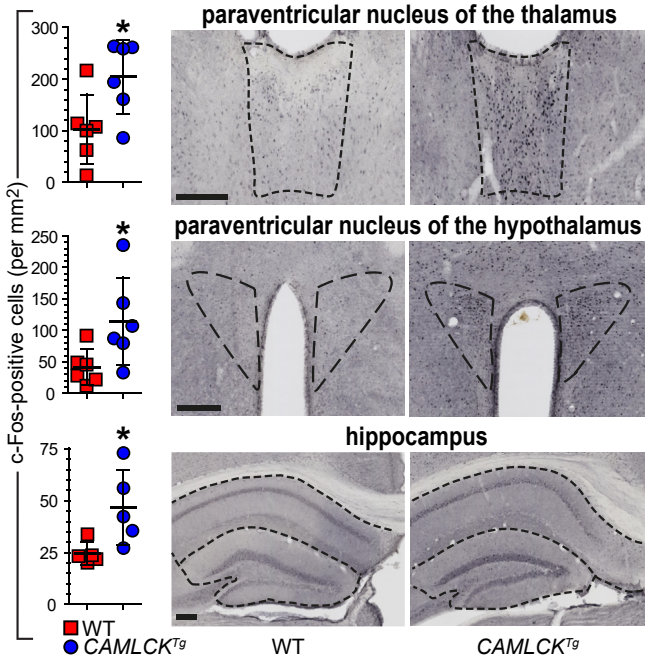

Figure 2. Increased intestinal permeability induces increased c-Fos immunolabeling in selected brain regions. *CAMLCK*^{Tg} (blue circles, n = 5–6) and WT (red squares, n = 5–6) littermates. Representative images of c-Fos–immunolabeled brains from *CAMLCK*^{Tg} and WT mice. Scale bars = 200 μm. Values are mean ± SD. *$P < .05$, *t* test.

O. INCZEFI[1,2,a]
V. BACQUIÉ[1,a]
M. OLIER-PIERRE[1]
M. RINCEL[3]
B. RINGOT-DESTREZ[4]
S. ELLERO-SIMATOS[1]
H. EUTAMÈNE[1]
C. BÉTOULIÈRES[1]
J. THOMAS[3]
J. LAINÉ[3]
L. GROS[3]
M. LÉVÊQUE[1]
R. LEONARD[4]
C. HARKAT[1]
C. ROBBE-MASSELOT[4]
R. RÓKA[2]
M. MERCIER-BONIN[1]
V. THEODOROU[1]
M. DARNAUDÉRY[3]
J. R. TURNER[5]
L. FERRIER[1]

[1]UMR 1331 ToxAlim, French National Institute for Agriculture, Food, and Environment, Toulouse, France
[2]First Department of Medicine, University of Szeged, Szeged, Hungary
[3]UMR 1286, Nutrition and Integrative Neurobiology, University of Bordeaux, French National Institute for Agriculture, Food, and Environment, Bordeaux, France
[4]Unité de Glycobiologie Structurale et Fonctionnelle, Université de Lille, Villeneuve d'Ascq, France; and
[5]Laboratory of Mucosal Barrier Pathobiology, Department of Pathology, Brigham and Women's Hospital, Harvard Medical School, Boston, Massachusetts

Address correspondence to: Laurent Ferrier, PhD, INRAE, UMR 1331 ToxAlim, 180 chemin de

Tournefeuille, 31027 Toulouse, France. e-mail: laurent.ferrier@inrae.fr; fax: +33 (0)5 61 28 52 44; or Jerrold R. Turner, MD, PhD, Harvard Medical School, Department of Pathology, 77 Avenue Louis Pasteur, NRB 730, Boston, MA 02115. e-mail: jrturner@bwh.harvard.edu.

References

1. Su L, et al. Gastroenterology 2009;136:551–563.
2. Edelblum KL, et al. Cell Mol Gastroenterol Hepatol 2017;4:285–297.
3. Meddings JB, et al. Gastroenterology 2000;119:1019–1028.
4. Yu D, et al. Proc Natl Acad Sci U S A 2010;107:8237–8241.
5. Rincel M, et al. Psychopharmacology (Berl) 2019;236:1583–1596.
6. Larauche M, et al. Neurogastroenterol Motil 2012;24, 1031-e547.
7. Guerrero-Alba R, et al. Gut 2017;66:2121–2131.
8. Witt ST, et al. Neuroimage Clin 2019;21:101602.
9. Larauche M, et al. Neurogastroenterol Motil 2019;31:e13489.
10. Ait-Belgnaoui A, et al. Psychoneuroendocrinology 2012;37:1885–1895.

[a]Authors share co-senior authorship

Most current article

2352-345X
https://doi.org/10.1016/j.jcmgh.2020.02.008

Received January 14, 2020. Revised February 26, 2020. Accepted February 27, 2020.

Conflicts of Interest

These authors disclose the following: Jerrold R. Turner is a cofounder of Thelium Therapeutics. The remaining authors disclose no conflicts.

Funding

This work was supported by an institutional grant from INRA and by National Institutes of Health grants R01DK61931 and R01DK68271 (to Jerrold R. Turner). Muriel Darnaudéry was supported by Bordeaux University, the FFAS (Fond Français Alimentation Santé), and the ANR (Agence Nationale de la Recherche). Marion Rincel was supported by the French ministry of research and education and Labex Brain. Julie Thomas was a recipient of a fellowship from the French Society of Paediatric Research. Orsolya Inczefi was a recipient of a fellowship from the Nutrition, Chemical Food Safety and Consumer Behaviour Division of INRA.

Supplementary Methods

Animals

CAMLCK^{Tg} mice[1–4] (Tg(Vil-FLAG-CAMLCK)#Jrt) were maintained as male heterozygotes on C57BL/6J background. These were mated with wild-type (WT) C57BL/6J female mice to produce WT and *CAMLCK*^{Tg} littermates. At weaning, female mice were separated and housed at constant temperature (22 ± 1°C) with a 12-hour light/dark cycle. Food (Teklad 2018; Envigo, Indianapolis, IN) and water were available ad libitum. All experiments were performed at 8 weeks of age. Procedures were approved by the Ethical Committee CEEA-86, under the number APAFiS#4145.

Gut Microbiota Composition Analysis

Gut microbiota were analyzed in two cohorts (15 WT and 16 *CAMLCK*^{Tg}) from 8 different WT dams. At sacrifice, colonic contents were stored at −80°C. DNA was extracted using the ZR fecal DNA MiniPrep kit (Zymo Research, Irvine, CA) and adjusted to 1 ng/μL. Changes in relative abundance of 24 microbial 16S rRNA gene targets were obtained by quantitative reverse-transcription polymerase chain reaction (PCR) using an adapted Gut Low-Density Array platform.[5–7] A universal bacterial primer set was included as the reference gene. quantitative reverse-transcription PCR was performed in duplicate on a ViiA7 (Applied Biosystems, Foster City, CA).

Fluorescence data were imported into LinRegPCR to perform baseline corrections, calculate mean PCR efficiency per amplicon group. and calculate initial quantities. Among the 24 targeted amplicon groups, 6 were not detected in any fecal samples and were removed from the analysis (*Bacteroides vulgatus*, *Alistipes spp*, *Parabacteroidetes distasonis*, *Roseburia spp*, *Escherichia coli*, and *Akkermansia muciniphila*). Normalized N_0-values were $\log_{10}$-transformed and processed by mixOmics (v6.1.1; https://www.bioconductor.org/packages/release/bioc/html/mixOmics.html) with RStudio (v1.0.44; RStudio, Boston, MA) to build a partial least-squares discriminant analysis. This multivariate supervised approach projects samples (X) onto a low-dimensional space of latent variables to maximize separation between groups according (Y = genotype). Leave-one-out cross-validation was used to select the optimal number of latent variables for partial least-squares discriminant analysis models.

Open Field Test

Mice explored a 50 × 50 cm arena (illumination 300 lx) for 10 minutes. Exploration was automatically assessed using a video tracking system (Bioseb, Vitrolles, France). The percentage of distance traveled and time spent and in the center area (20 × 20 cm) and total distance traveled in the entire arena were assessed.

Colorectal Distension

Two 0.08-mm diameter electrodes were implanted in the abdominal external oblique muscle and a third in the abdominal skin. On postoperative days 3–6, colorectal distension (CRD) was performed using a balloon catheter (Fogarty 4F catheter [Edwards Lifesciences, Irvine, CA], 1.1 cm length, tip 3.5 cm from the anus)[8] in 10-second periods with increasing volumes from 0.02 mL to 0.10 mL, with 5 minutes' rest between distensions. Abdominal electromyography activity was registered after the amplification (10,000×) and analyzed (Powerlab Chart 5; ADInstruments, Sydney, Australia). Basal electromyographic activity was subtracted from electromyographic activity registered during distension. Some mice were treated with ML-7 (2 mg/kg intraperitoneal) or naloxone sulfate (2 mg/kg intraperitoneal) 1 hour before CRD. For others, water avoidance stress was induced on a floating platform (3 × 3 cm) in the middle of a water-filled tank (40 × 40 cm) for 1 hour daily over four days. Recovery (30 minutes) preceded CRD.

Gastrointestinal Transit

Animals received 70 μL of 100-mg/mL TRITC-70kDa dextran in tap water by gavage and were sacrificed 1 hour later.[9] The stomach and small and large intestine were cut in 11 equal parts. Luminal contents of each segment were centrifuged and fluorescence determined. Transit was calculated as the geometric center of the values for each mouse.

Ussing Chamber Analysis

Jejunal sections were mounted in Ussing chambers (Physiologic Instruments, San Diego, CA) filled with Krebs buffer and continuously oxygenated (95% O_2, 5% CO_2). After 1 hour of equilibration, fluorescein (1 mg/mL) was added in the apical chamber and fluorescence intensity of the basolateral chamber was measured after 1 hour.

In Vivo Permeability Analysis

Mice were fasted for 4 hours before gavage with 150 μL of 100-mg/mL FITC-4kDa dextran in tap water. Blood (200 μL) was collected after 4 hours and plasma fluorescence determined.

C-Fos Analysis

Vibratome sections (40 μm) were stained using polyclonal rabbit anti-c-Fos (Santa Cruz Biotechnology, Dallas, TX) and secondary horseradish peroxidase–conjugated goat anti-rabbit antisera (Jackson ImmunoResearch, West Grove, PA). NDPI images (×20) were obtained (Nanozoomer; Hamamatsu Photonics, Hamamatsu, Japan) and converted into TIFF format using ImageJ (NDPI tools plugin; National Institutes of Health, Bethesda, MD; https://imagej.nih.gov/ij, version 1.52a). Regions of interest were manually circumscribed using region-of-interest tools and c-Fos–immunoreactive cells quantified automatically using the particle analysis function (size: 5–20 μm^2; circularity: 0.5–1). For each animal, 3–6 sections of each brain area were assessed by a blinded observer.

Statistical Analysis

Statistical significance was determined by 2-tailed *t* test, 2-tailed Mann-Whitney *U* test, or 2-way analysis of variance and set at $P < .05$. For microbial analyses, univariate analysis was realized in parallel to compare each amplicon separately using unpaired *t* test followed by the Benjamini-Hochberg adjustment of *P* values for multiple comparisons.

Supplementary References

1. Su L, et al. Gastroenterology 2009;136:551–563.
2. Weber CR, et al. J Biol Chem 2010;285:12037–12346.
3. Edelblum KL, et al. Cell Mol Gastroenterol Hepatol 2017;4:285–297.
4. Yu D, et al. Proc Natl Acad Sci U S A 2010;107:8237–8241.
5. Bergstrom A, et al. FEMS Microbiol Lett 2012;337:38–47.
6. Bergstrom A, et al. Appl Environ Microbiol 2014;80:2889–2900.
7. Riba A, et al. Gastroenterology 2017;153:1594–1606.e2.

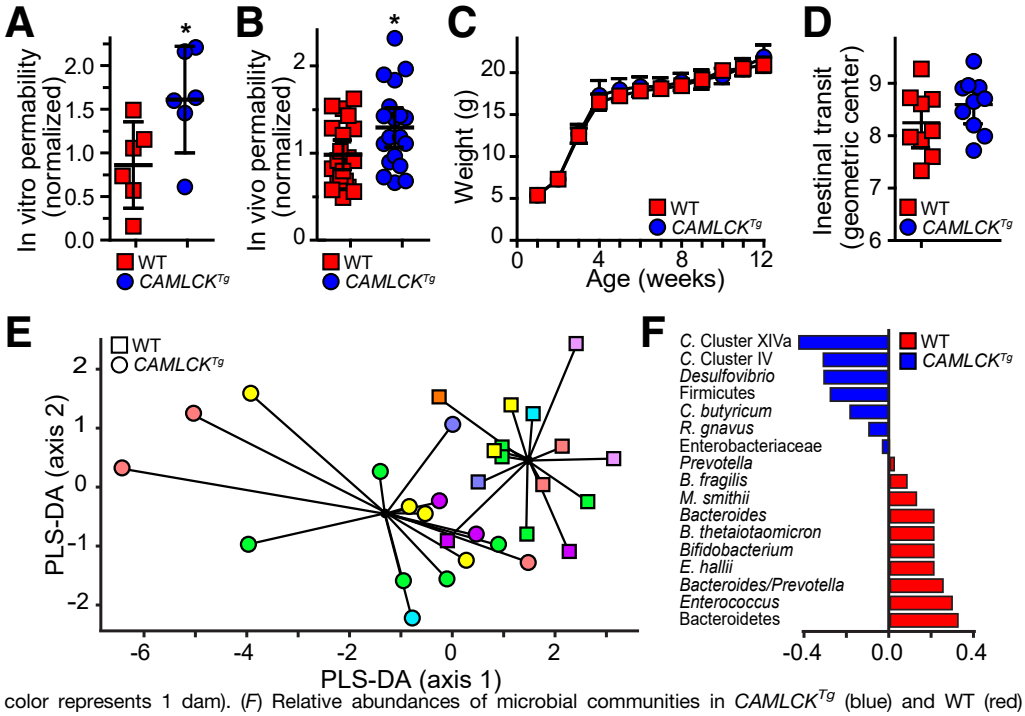

Supplementary Figure 1. (*A*) Transjejunal fluorescein flux was increased in *CAMLCK*^{Tg} (blue circles) relative to wild-type (WT) (red squares) littermates. Values are mean ± SD. **P* < .05. Mann-Whitney *U* test. (*B*) In vivo analysis using FITC-4kDa dextran demonstrated increased permeability of *CAMLCK*^{Tg} (blue circles, n = 19) relative to WT (red squares, n = 20) littermates. Values are mean ± SD. **P* < .05, *t* test. (*C*) Weight gain was similar in WT (red squares, n = 6) and *CAMLCK*^{Tg} (blue circles, n = 6) littermates. Values are mean ± SD. (*D*) Intestinal transit was similar in WT (red squares, n = 10) and *CAMLCK*^{Tg} (blue circles, n = 9) littermates. Values are mean ± SD. (*E*) Partial least-squares discriminant analysis (PLS-DA) score plot based on the relative abundances of 18 microbial taxa in gut contents of *CAMLCK*^{Tg} (circles, n = 16) and WT (squares, n = 15) born to 8 different dams (each color represents 1 dam). (*F*) Relative abundances of microbial communities in *CAMLCK*^{Tg} (blue) and WT (red) mice. Diagrams indicate regions analyzed.

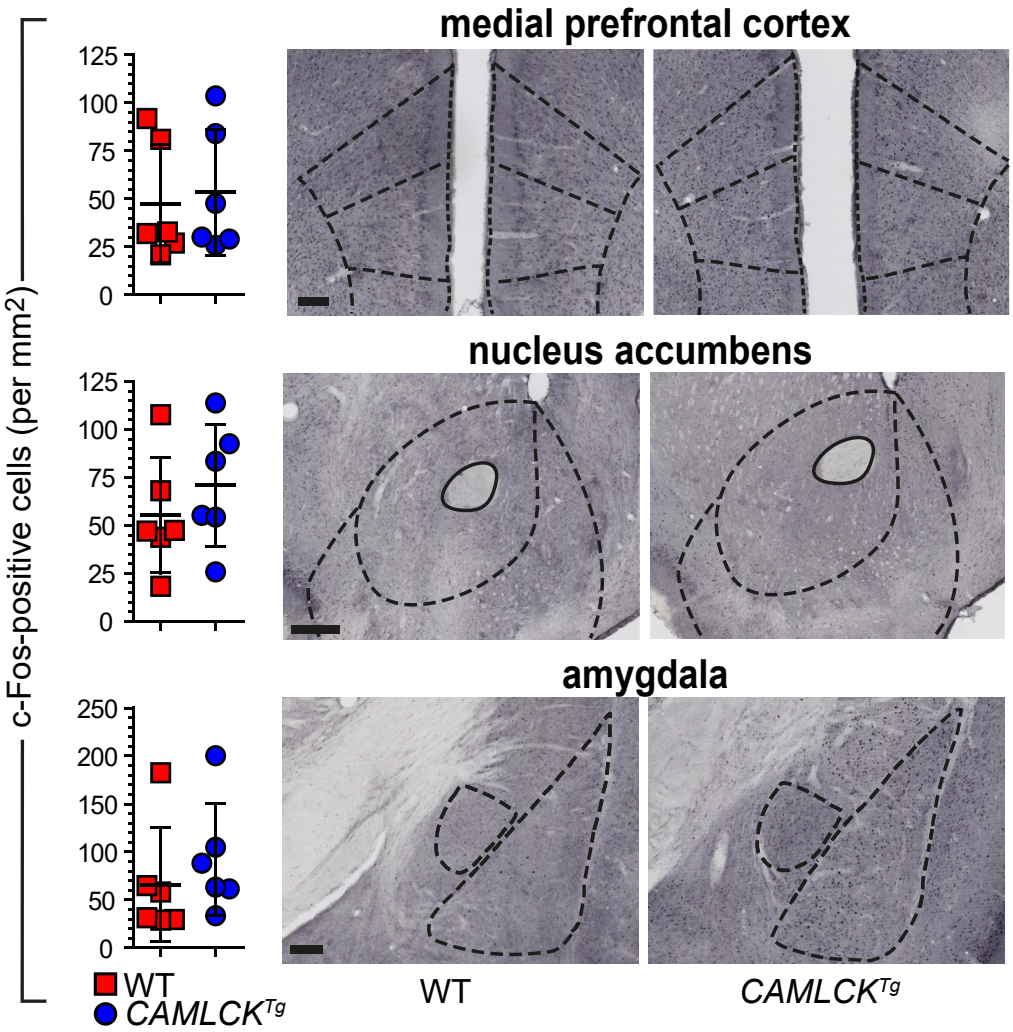

Supplemental Figure 2. *CAMLCK*^{Tg} (blue circles, n = 5–6) and wild-type (WT) (red squares, n = 5–6) littermates. Representative images of c-Fos–immunolabeled brains from *CAMLCK*^{Tg} and WT mice. Scale bars = 200 μm. Values are mean ± SD. *$P < .05$, *t* test.